Structure and Properties of Mn_n, Mn_n^-, and Mn_n^+ Clusters ($n = 3-10$)

G. L. Gutsev* and M. D. Mochena

Department of Physics, Florida A & M University, Tallahassee, Florida 32307

C. W. Bauschlicher, Jr.

Mail Stop 230-3 NASA Ames Research Center, Moffett Field, California 94035

Received: April 25, 2006; In Final Form: June 12, 2006

Electronic and geometrical structures of Mn_3-Mn_{10} together with their singly negatively and positively charged ions are computed using density functional theory with generalized gradient approximation. The ground-state spin multiplicities in the neutral series are 16, 21, 4, 9, 6, 5, 2, and 5, for Mn_3-Mn_{10}, respectively. Thus, there is a transition from a ferromagnetic ground state to a ferrimagnetic ground state at Mn_5. The energy difference between ferrimagnetic and ferromagnetic states in Mn_n grows rapidly with increasing n and exceeds 2 eV in Mn_{10}. The corresponding change from ferro- to ferrimagnetic ground state occurs at Mn_6^- and Mn_3^+ in the anionic and cationic series, respectively. Beginning with Mn_6, the ion spin multiplicities differ from that of the neutral by ± 1 (i.e., they obey the empirical "± 1 rule"). We found that the energy required to remove an Mn atom is nearly independent of the charge state of an Mn_n cluster and the number of atoms in the cluster, except for Mn_3. The results of our calculations are in reasonable agreement with experiment, except for the experimental data on the magnetic moments per atom, where, in general, we predict smaller values than the experiment.

I. Introduction

The most stable polymorph of Mn under normal temperature and pressure, α-Mn, exhibits an exotic crystalline structure with 58 atoms per a cubic unit cell and is antiferromagnetic. Although the net total magnetic moment is zero, the local magnetic moments at the atoms in α-Mn vary[1] in the absolute value from 0 to ∼3 Bohr magneton (μ_B), depending on the site symmetry. On the contrary, the Mn_5 cluster was found to have 25 unpaired electrons in electron-spin-resonance (ESR) studies,[2,3] which yields the total magnetic moment of $25\mu_B$. Such a difference between the bulk and cluster magnetic properties leads to a question: which Mn_n clusters possess high-spin ferromagnetic ground states and at what size do the clusters transition to low-spin ferrimagnetic states? Early calculations[4] using density functional theory with generalized gradient corrections for the exchange-correlation functional (DFT-GGA) found that the Mn_2, Mn_3, Mn_4, and Mn_5 ground states are ferromagnetic and possess the total magnetic moments of $10\mu_B$, $15\mu_B$, $20\mu_B$, and $25\mu_B$, respectively. Another DFT-GGA study,[5] which appeared shortly after, extended the series of clusters possessing ferromagnetic ground states to Mn_6, Mn_7, and Mn_8, with the total magnetic moments of $26\mu_B$, $29\mu_B$, and 32 μ_B, respectively.

However, the results of recent DFT-GGA calculations[6] suggest that the antiferromagnetic ordering is preferable beginning with Mn_5, whose lowest-energy ferrimagnetic state (with a total magnetic moment of $3\mu_B$) is below the lowest ferromagnetic state (with the total magnetic moment of $23\mu_B$) by 0.05 eV. It was also found that the energy gap between the ferri- and ferromagnetic states grows from 0.03 eV in Mn_6 to 0.63 eV in Mn_7 and 2.42 eV in Mn_{13}. A subsequent study[7] of Mn_5 and Mn_6 supported this view, finding ferrimagnetic ground states with the spin multiplicities $2S+1 = 4$ and $2S+1 = 9$, respectively; these spin multiplicities correspond to the same total magnetic moments as obtained by Bobadova-Parvanova et al.[6] (under a commonly accepted assumption that 2S is the value of the total magnetic moment expressed in μ_B). A DFT-GGA study[8] of Mn_7 found its ground state to be ferrimagnetic with the spin multiplicity $2S+1 = 6$, which corresponds to the total magnetic moment of $5\mu_B$, as obtained by Bobadova-Parvanova et al.[6] The larger Mn_8, Mn_9, Mn_{12}, and Mn_{13} clusters were recently found[9] to have the total magnetic moments of $4\mu_B$, $9\mu_B$, $12\mu_B$, and $3\mu_B$, respectively. However, some of these values were obtained from calculations that considered only total spins that were consistent with the experimental value including its uncertainty.[9] A previous DFT-GGA study[10] of Mn_{13} predicted the icosahedral geometry for the lowest total energy state as well but obtained a significantly larger total magnetic moment of $33\mu_B$.

Kawazoe et al.[11] used a plane-wave method, employing ultra soft pseudopotentials and a GGA for the exchange-correlation potential, to optimize the geometrical structures of Mn_{13}, Mn_{15}, Mn_{19}, and Mn_{23} and estimated the local magnetic moments by integrating the spin density over Voronoi cells. They also obtained a total magnetic moment of 3 μ_B for the lowest-energy icosahedral state of Mn_{13}, which is somewhat smaller than the experimental value[12] of 7.28 ± 1.69 μ_B.

Deviations in the symmetry of the electronic densities from the symmetry imposed by the corresponding crystal lattices found in some ferro- and ferrimagnetic states led to the notion of noncollinear magnetism (NCM) and modifications of the existing band structure computation codes.[13,14] In the NCM approach, the valence electrons are not only separated into the spin-up and spin-down moieties but also the excess spin densities, resulting in the local magnetic moments at the atoms,

* Corresponding author. E-mail: gennady.gutsev@famu.edu.

10.1021/jp062533l CCC: $33.50
Published on Web 07/15/2006

which may have orientation axes that are not parallel to each other. Computations using a NCM local-spin density approximation (LSDA) band-structure code were performed on super-cells containing Mn_6[15] and Mn_2-Mn_7.[16] These computations predicted the existence of "magnetically noncollinear isomers that are more stable than the collinear structures."[16] However, it was previously found[17] in computations of small Cr and Fe clusters that "gradient corrections are absolutely essential in predicting the correct magnetic ground states of small clusters."[17] After adding the GGA corrections, only "some very slight distortion of the density in the noncollinear Fe_5 ground-state structure" was found.[17]

Our experience on transition metal clusters suggests that a description that allows localized 3d orbitals is superior to one that imposes the point-group symmetry of the nuclear frame and thus forces a delocalized description. Hence, imposing no symmetry constraints is critical in obtaining the best description of many transition metal clusters. The results of recent computations[18] of collinear magnetism in iron clusters lend support to this point of view. It was concluded[18] that "the full relaxation of the atoms without imposing any symmetry constraints leads to unsymmetrical arrangements of the atoms (distorted clusters) and restores collinearity of the magnetic moments of all clusters considered so far".

Mn is considered[19] as a prospective dopant of semiconductor materials for their conversion into a ferromagnetic phase. One of the most actively studied systems is a $Ga_{1-x}Mn_xAs$ diluted magnetic semiconductor, which becomes ferromagnetic[20-22] at 110 K for $x \approx 0.05$. Recently, it was found[23] that dopant Mn atoms may form clusters, which can seriously influence the magnetic properties with respect to those samples that possess a uniform Mn monomer distribution. Mn clusters in semiconductors may be in charged states because the experimental data[24] on ionization energies (IE) of Mn_n clusters, $n = 7-64$, show that the IE values do not exceed 5.44 eV in this series. Our preliminary computations show that Mn_3 carries a charge of $+0.5$ e in a $(GaAs)_4Mn_3$ cluster.

Ionized Mn_n clusters are less studied than the neutrals. Among the Mn_n ions, the dimers Mn_2^- and Mn_2^+, whose ground states were found to be $^{10}\Sigma_g^-$ and $^{10}\Pi_u$, respectively, have received[25] the most attention. The ground states of Mn_5^- and Mn_6^- were computed[7] to have $2S+1 = 23$ and $2S+1 = 8$, respectively. Optical spectra were measured[26] for the Mn_3^+ trimer, and dissociation energies were measured[27,28] for $Mn_2^+-Mn_7^+$.

This work is aimed at the search of the ground and lowest excited states of the Mn_n^- and Mn_n^+ clusters, $n = 3-10$, and estimating their thermodynamic stability. Simultaneously, we performed extensive optimizations of the neutral Mn_n clusters to obtain their ground-state total energies and compute the electron affinities, ionization energies, and dissociation energies in the neutral series. Natural atomic populations on atoms are used to gain insight in the antiferromagnetic coupling in ferrimagnetic states. As with the neutrals, it is very interesting to compare the high- and low-spin states as a function of cluster size for the ions.

II. Computational Details

Computations were performed using the Gaussian 98[29] and Gaussian 03[30] program systems. We used the 6-311+G* basis set[31-34] of Mn (15s11p6d1f)/[10s7p4d1f]. As in our previous work, we choose the BPW91 method, where the exchange-correlation functional is comprised of the Becke's exchange[35] and Perdew-Wang's correlation,[36] because, although similar results are obtained with many of the functionals, the BPW91 vibrational frequencies of the Fe_n clusters are found[37] to be less sensitive to the grid used in the numerical integration than those computed by some of the other functionals incorporated into Gaussian 98 and 03. Therefore, smaller integration grids can be used for the BPW91 approach, which makes this method computationally less demanding.

Geometry optimizations of ferrimagnetic states are rather complicated. In many cases, optimizations started with the default electronic densities did not converge. While switching from Gaussian 98 to Gaussian 03 improved the convergence of the ferrimagnetic states, we found it superior to avoid using the default guess except for the high spin states. Usually, the optimal strategy is to first optimize a high-spin state where each atom contributes 5 unpaired electrons, then to decrease the number of unpaired electrons by two and converge that state, and repeat the process of decreasing the number of unpaired electrons until a singlet (even-n Mn_n clusters) or doublet state is reached. We used this process for the neutrals, cations, and anions. Several additional tests were performed to ensure than we have found the lowest state for each spin. These include new optimizations starting from a converged solution and increasing the number of unpaired electrons by two. This is essentially the reverse of the first process, but sometimes allows one to find a lower-energy solution. Another test is to take the orbitals from a cluster with a different charge and change the number of unpaired electrons by one. For example, to take an anion solution with $2S+1 = m$ and use it as a starting point for an optimization of the neutral with $2S+1 = m+1$ or $m-1$. When this switching between "neighbor series" finds a new solution, one naturally uses this as a starting point for increasing and decreasing the number of unpaired electrons. This procedure is followed until it appears that one has found the lowest energy state for each spin.

All optimizations, except some for the Mn_3 series, were performed without imposing any symmetry constraints. Each geometry optimization was followed by an analytical second derivatives calculation of the harmonic vibrational frequencies to confirm that the optimized geometry corresponds to a minimum. Rather often, the optimizations arrived at transition states, and the vibrational modes of the corresponding imaginary frequencies were used for the generation of a guess geometry used in the subsequent reoptimizations.

Our reported electron affinities and ionization energies are computed as the differences in total electronic energies corrected for the zero-point vibrational energies (ZPVE) and correspond to adiabatic values. Fragmentation energies, computed as the differences in total energies of the species and their decay constituents, are corrected for the ZPVEs. We compute atomic spin densities using both Mulliken[38] and natural atomic orbital (NAO)[39] approaches. Generally, the values obtained in the both approaches are nearly the same.

III. Results and Discussion

A. Geometries and Chemical Bonding. In this section, we discuss the results of geometry optimizations of the neutral and charged series. The nature of the chemical bonding is described using the NAO analysis. The influence of symmetry constraints was considered for the Mn_3 series, whereas we use only symmetry-unconstrained computations for Mn_4-Mn_{10}.

We first consider Mn_2, which has been published previously.[25,40] The Mn ground state is $^6S(3d^54s^2)$. Thus, if the ground state of Mn_2 were derived from two ground-state Mn atoms, it would be a van der Waals molecule with a $^{11}\Sigma^+_g$ or $^1\Sigma^+_g$ ground state. Promotion from the 4s orbital to a vacant 3d orbital allows

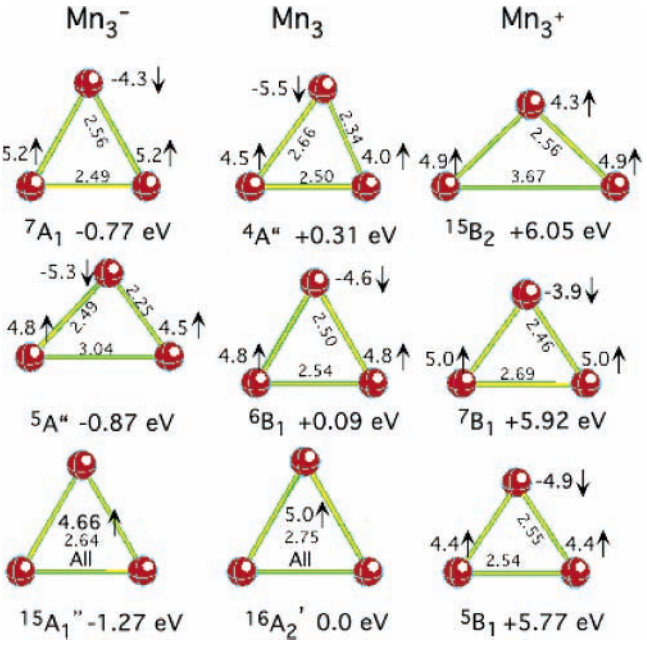

Figure 1. Optimized ferro- and ferri-magnetic states of Mn_3, Mn_3^-, and Mn_3^+. Bond lengths are in Å, excess spin densities in electrons.

some 4s−4s covalent bonding, but the experimental[41] $3d^54s^2 \rightarrow 3d^64s^1$ excitation energy for Mn is 2.15 eV, the highest in the 3d-atom series. Given this large promotion energy, it is clear that both Mn atoms will not have a $3d^64s^1$ occupation, and we found a $^{11}\Pi_u$ ground state, where only one Mn has promoted a 4s electron to the 3d orbital. In this state, the two 3d α-shells are filled and are nonbonding. There are two electrons in the 4s α-orbitals, which are also nonbonding. The 3d and 4s orbitals in the α-spin representation of Mn_2 produce no net bonding because all the bonding and antibonding α-orbitals are occupied. In the NAO view, they are classified as nonbonding localized spin−orbitals (LSOs). Two bonds are formed in the β-spin representation, namely, one 4s+4s and one 3dπ+3dπ bond. Unlike DFT, some traditional methods, such as second-order perturbation theory, do not predict[42] a 4s to 3d promotion for the ground state of Mn_2. Although it is possible that the DFT prediction of such a promotion for Mn_2 is incorrect, it is clear that more and more 4s to 3d promotions should occur as the Mn_n cluster size increases, and we monitor this promotion as a function of the cluster size in our analysis of the bonding in these clusters.

1. Mn_3, Mn_3^-, and Mn_3^+. We performed first an extensive search of the lowest energy states for each spin multiplicity of Mn_3, Mn_3^-, and Mn_3^+ without imposing any symmetry constraints. Next, we imposed the symmetry constraints according to the symmetry of the nuclear framework and reoptimized the corresponding states. In those cases where the reoptimization led to the same geometrical structures and total energy as found in the calculations with no symmetry constraints, the states are identified using the higher symmetry notation. Optimized structures of the ground and two lowest excited states of Mn_3, Mn_3^-, and Mn_3^+ are presented in Figure 1. In agreement with the previous work,[4−6,43] the ground state of Mn_3 is ferromagnetic and has the spin multiplicity $2S+1 = 16$, which corresponds to the total magnetic moment of 15 μ_B. The lowest excited states of Mn_3, with $2S+1 = 4$ and $2S+1 = 6$, are ferrimagnetic, and their reduced symmetry reflects the antiparallel spin coupling in these states.

Attachment of an extra electron to an a_2'' orbital results in the $^{15}A_1''$ ground state of Mn_3^-, whereas the detachment of an electron leads to a rather surprising result. The $^5B_1$ ground state of Mn_3^+ is ferrimagnetic, whereas the lowest ferromagnetic state $^{15}B_2$ is 0.28 eV above the ground state, see Figure 1. Using a hybrid functional[26] yields a ferromagnetic $^{17}B_2$ ground state of Mn_3^+ with the bond length of 3.03 Å and an apex angle of 144°. Starting with this geometry, we optimized a $^{17}B_2$ state using our BPW91/6-311+G* approach and found that it converged to a $^{17}B_2$ state with the bond length of 2.83 Å and the apex angle of 70.6°. This $^{17}B_2$ state is above the $^5B_1$ ground state by 0.41 eV. Generally, it is not recommended[37,44] to use hybrid methods in transition-metal cluster computations, as they do not appear to describe metal−metal bonds as accurately as pure functionals.

Let us consider the changes in the atomic populations of the Mn_3 ground state due to the attachment and detachment of an electron. The total valence NAO populations in the neutral ground state (neglecting contributions of 4p states that are less than 0.1 e) are $3d^{5.54}4s^{1.39}$ on each atom and consist of the $\mathbf{3d^{5.00}4s^{0.97}}$ and $3d^{0.54}4s^{0.42}$ contributions from the α- and β-spin representations, respectively. Note that the spin−orbitals that are completely occupied are given in bold. One can see the promotion of about a half of a 4s-electron per Mn atom to vacant 3d orbitals, which is similar to the promotion found for Mn_2. Such NAO populations correspond to the formation of three 3d−4s hybrid bonding orbitals in the β-spin representation, whereas all valence α-electrons occupy nonbonding LSOs, as in Mn_2. Attachment of an extra electron does not affect the α-population whereas the β-population becomes $3d^{0.67}4s^{0.56}$. That is, the extra electron contributes nearly equally to the 3d and 4s β-populations, and the number of β-bonds increases by one.

A NAO analysis of the Mn_3^+ $^5B_1$ state shows that the excess spin density on the apex atom is antiferromagnetically coupled to the excess spin densities of two basal atoms. The total atomic populations in the $^5B_1$ state are $3d^{5.52}4s^{0.91}$ and $3d^{5.70}4s^{0.93}$ on the apex and basal atoms, respectively. The α-contribution consists of one atom with a $3d^{0.61}4s^{0.21}$ occupation and two with $\mathbf{3d^{4.93}}4s^{0.62}$, and the β-contribution consists of one atom with a $\mathbf{3d^{4.91}}4s^{0.70}$ occupation and two with $3d^{0.78}4s^{0.31}$. Comparing these populations with those in the neutral, one can see that flipping the spin of electrons in the half-filled 3d-shell of the apex atom results in the excess spin density of this atom being antiparallel to the excess spin densities of the basal atoms. We label the ferrimagnetic states as "n_1:n_2", where n_1 is the number of atoms possessing the excess spin densities of one sign and n_2 is the number of atoms possessing the excess spin densities of the opposite sign; clearly the two sets are antiferromagnetically coupled to each other. Thus the $^5B_1$ state has the 1:2 ordering. The antiferromagnetic coupling in this 1:2 state allows the formation of $4s_{base1}+3d_{apex}+4s_{base2}$ α-bonds and $3d_{base1}+4s_{apex}+3d_{base2}$ β-bonds.

Relative to the ground state of Mn_3, the high-spin ferromagnetic state $^{15}B_2$ of the Mn_3^+ cation is formed by detaching an electron from an α-4s LSO of the neutral. The β-contribution of the cation NAO has some C_{2v} distortion, but, like the neutral, there are three 3d4s hybrid bonds. The α-contribution consists of one atom with $\mathbf{3d^{4.99}}4s^{0.45}$ and two with $\mathbf{3d^{4.99}}4s^{0.77}$. An inspection of the orbitals shows that 3d orbitals are nonbonding and there are two occupied 4s derived orbitals, namely a delocalized 4s+4s+4s bond and an antibonding $4s_{basal1}$-$4s_{basal2}$ orbital. Thus, the bonding in the 1:2 ferrimagnetic $^5B_1$ state is energetically preferable since there are two α-bonds.

2. Mn_4, Mn_4^-, and Mn_4^+. Consistent with the previous work,[4−6] the ground state of neutral Mn_4 is ferromagnetic with

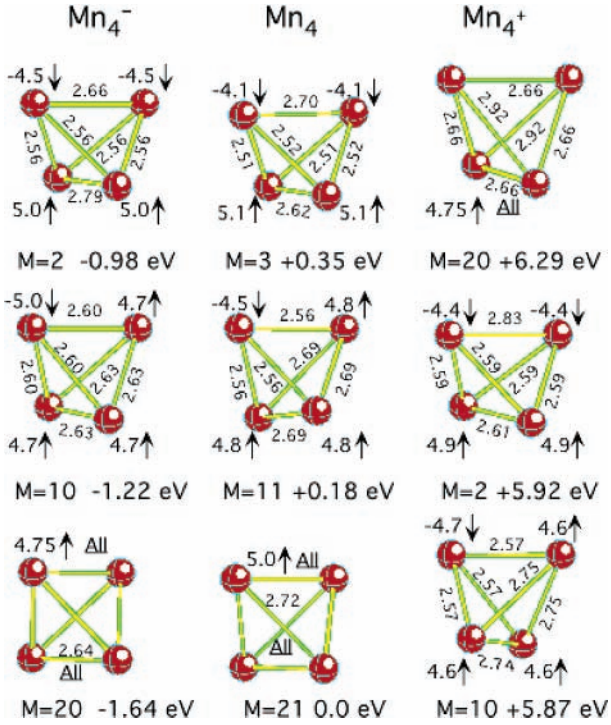

Figure 2. Optimized states of Mn_4, Mn_4^-, and Mn_4^+.

a spin multiplicity of 21. The ground-state geometry is tetrahedral, see Figure 2, and the total atomic populations for the four equivalent atoms are $3d^{5.55}4s^{1.33}$, which are similar to those in Mn_3. Attachment of an extra electron results in the ferromagnetic ground state with $2S+1 = 20$, a tetrahedral geometry, and the total atomic populations of $3d^{5.66}4s^{1.46}$. Detachment of an electron leads to the 1:3 ferrimagnetic ground state with a spin multiplicity of 10. Note that the distance between the spin-up atoms is 2.75 Å whereas the distance between the spin-up and spin-down atoms is 2.57 Å. A 2:2 ferrimagnetic state is only 0.05 eV higher in total energy, whereas the lowest ferromagnetic state with $2S+1 = 20$ is higher by 0.42 eV, see Figure 2.

The bonding in the ground ferromagnetic states of Mn_4 and Mn_4^- is similar to that in the ferromagnetic states of the Mn_3 series; i.e., there are no bonds in the α-spin representation, which is presented by 6 LSOs per atom ($3d^54s^1$) and four and five β-3d4s-bonds in Mn_4 and Mn_4^-, respectively. In the ground 1:3 state of the Mn_4^+ cation, the α populations are: one atom with $3d^{0.71}4s^{0.18}$ and three atoms with $\mathbf{3d^{4.94}}4s^{0.71}$, whereas the β populations are: one atom with $\mathbf{3d^{4.87}}4s^{0.63}$ and three with $3d^{0.66}$-$4s^{0.41}$. There are four chemically inert half-filled 3d shells, three with α spin and one with β spin. The remaining 3d and 4s electrons form three one-electron bonds with α spin and four with β spin. For the 2:2 state, the α populations are: two atoms with a $3d^{0.70}4s^{0.54}$ occputation and two with $\mathbf{3d^{4.91}}4s^{0.66}$, whereas the β populations are: two atoms with $\mathbf{3d^{4.90}}4s^{0.65}$ and two with $3d^{0.63}$ $4s^{0.24}$. Again, each atom possesses an inert 3d-subshell, and there are seven one-electron bonds, four with α spin and three with β spin. That is, these two nearly degenerate states possess the same number of bonds.

3. Mn_5, Mn_5^-, and Mn_5^+. The lowest energy state of Mn_5 is a 2:3 ferrimagnetic state with $2S+1 = 4$ in agreement with previous computations.[4−6] The total magnetic moment per atom in this state is 0.6 μ_b, which agrees with the experimental value[12] of 0.79 ± 0.25 μ_b to within its error bars. We find that the lowest ferromagnetic state is 0.09 eV higher in energy, see Figure 3. In the ground state, the excess spin density of the

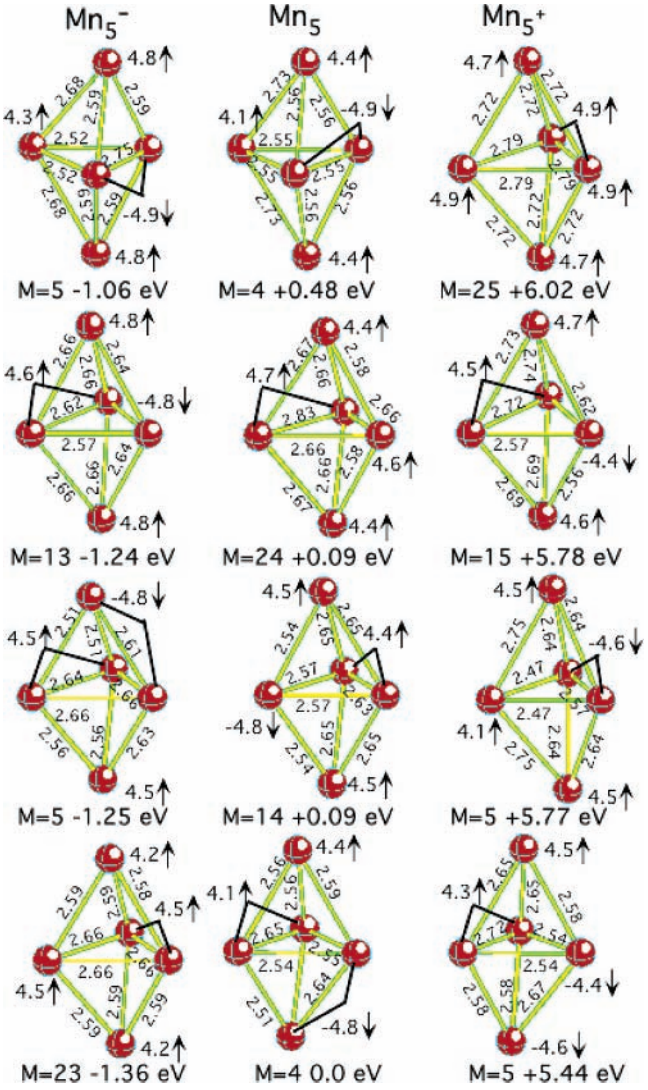

Figure 3. Optimized states of Mn_5, Mn_5^-, and Mn_5^+.

apex atom at the bottom of the cluster is parallel to the excess spin density of one of the atoms in the basal plane, and they both are antiferromagnetically coupled to the three others. A 2:3 $2S+1 = 4$ isomer, in which the two apex atoms and one of basal plane atoms are high-spin coupled, is 0.48 eV above the ground state.

An analysis of the NAO populations shows that there are 4 α-bonds and 4 β-bonds in the ground state of Mn_5, whereas the isomer has one fewer β-bond. Similar isomers are found for the cation and anion states with $2S+1 = 5$. The existence of isomers with the same spin multiplicity but with different couplings of the inert open-shell 3d electrons on different Mn atoms complicates a search for the ground state. We found no 2:3 ferrimagnetic states where the excess spin density of the two pyramidal atoms is antiferromagnetically coupled to the excess spin density of the basal atoms. This is in line with our results for the other Mn_n clusters, where atoms with the parallel excess spin densities are bonded, or, in other words, they form a connected set. Such a partitioning into two connected sets of atoms, with parallel excess spin densities on atoms in each set, reflects the specific chemical bonding in ferrimagnetic states; namely, there is 3d4s bonding within each set and a delocalized 4s-bonding between the two sets.

The Mn_5^- ground state is ferromagnetic and is below the lowest ferrimagnetic state by 0.11 eV. Its NAO populations are

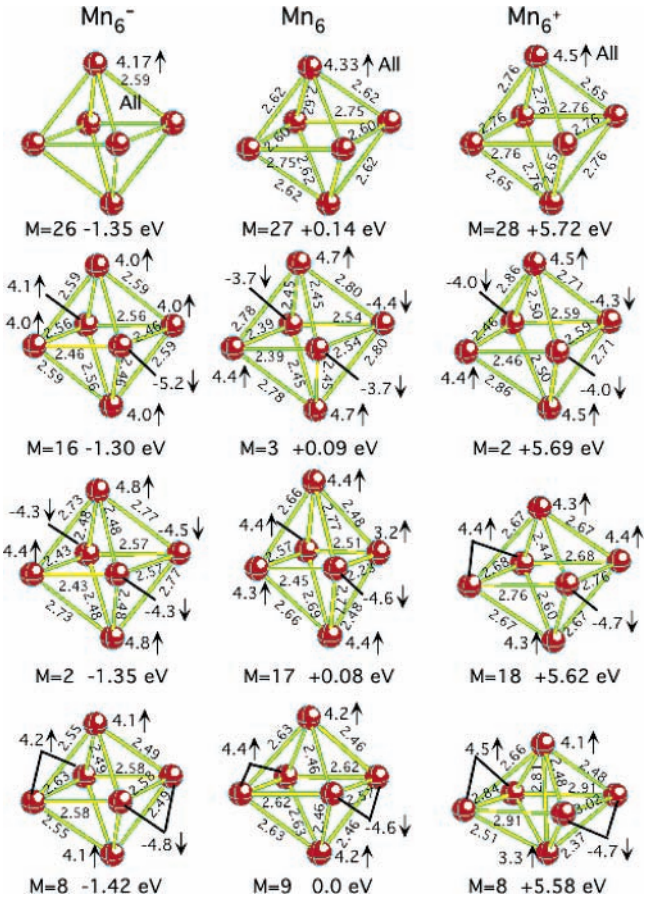

Figure 4. Optimized states of Mn_6, Mn_6^-, and Mn_6^+.

similar to that of the $^{15}B_2$ state of Mn_3^+: promotion of two 4s electrons into vacant 3d orbitals allows the formation of six β-3d4s bonds that appears to be more favorable than the formation of fewer 3d4s bonds, but divided between the two spin representation, in a ferrimagnetic state.

4. Mn_6, Mn_6^-, and Mn_6^+. In agreement with the previous work,[6,7] the ground state of Mn_6 is ferrimagnetic with $2S+1 = 9$ that corresponds to the total magnetic moment per atom of 1.33 μ_b, which is significantly larger than the experimental value[12] of 0.55 $\pm$ 0.10 μ_b. The lowest energy isomers of Mn_6 and Mn_6^-, shown in Figure 4, have the same ordering in total energy as found by Jones et al.[7] except for the reversal of the $Mn_6(2S+1 = 27)$ and $Mn_6(2S+1 = 3)$ states. Jones et al.[7] used an integration of excess densities in spheres around atoms; therefore, their corresponding excess spin densities are somewhat different from those shown in Figure 4.

Contrary to the Mn_3, Mn_4, and Mn_5 series, the ground-state multiplicities of Mn_6^- and Mn_6^+ obey the usual rule that the ground-state spin multiplicity of a singly charged ion differs from the ground-state multiplicity of the corresponding neutral by ± 1, which is usually an indication of a single-electron character of the detachment/attachment process. Mn_6 is not unique in this regard, as the ± 1 rule holds also for the series Mn_7-Mn_{10}. Thus, it appears that the ± 1 rule is violated only for the small clusters.

The ground state of Mn_6 possesses three pairs of atoms that have different excess spin densities. The total NAO populations (neglecting populations of 4p and higher AOs) are $3d^{5.78}4s^{1.15}$, $3d^{5.68}4s^{1.02}$, and $3d^{5.88}4s^{1.12}$, yielding the excess spin densities of 4.4, 4.6, and 4.2, respectively. The 3d population for all three pairs is closer to six, showing that most of the atoms have promoted a 4s electron into the 3d orbital. As for the previous

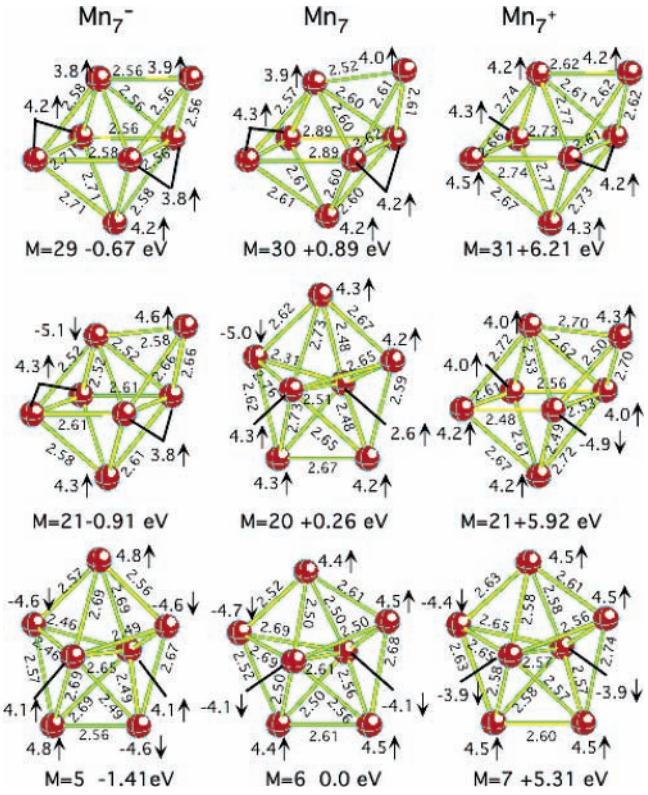

Figure 5. Optimized states of Mn_7, Mn_7^-, and Mn_7^+.

clusters, there is a chemically inert half-filled 3d shell on each atom. The remaining electrons form five bonds of α spin and seven of β spin. In the ferromagnetic $2S+1 = 26$ state, the total atomic populations are: four atoms with $3d^{5.80}4s^{1.06}$ and two with $3d^{5.86}4s^{1.09}$; thus, there is also a significant 4s to 3d promotion. There are 4 α- and 8 β-bonds; that is, the total number of bonding orbitals in the $2S+1 = 9$ and $2S+1 = 26$ states is the same, and these two states are separated by only 0.14 eV.

5. Mn_7, Mn_7^-, and Mn_7^+. The ferrimagnetic ($2S+1 = 6$) ground state of Mn_7 is a pentagonal bipyramid (see Figure 5), in agreement with the previous results;[8,9] however, the spin-down excess spin densities are located on different atoms in all three works. This appears to be due to small energy changes between isomers with 3:4 couplings. Unfortunately, it is not straightforward to obtain all possible isomers with a 3:4 coupling because we can do it only indirectly by changing the bond lengths, as it is not possible to create starting densities by flipping the excess spin densities on specific atoms. Note that the magnetic moment per atom for the ground state is 0.71 μ_b, which compares favorably with the experimental value[12] of 0.72 $\pm$ 0.42 μ_b.

There are several low-lying excited states with the spin multiplicities of 8 (+0.08 eV), 10 (+0.15 eV), and 14 (+0.17 eV) that have the geometries similar to that of the ground state. These low-lying states are not shown in Figure 5, but rather we jump to some states with larger spin multiplicities, for example, a $2S+1 = 20$ state that has the lowest total energy among the 1:6 isomers. Beginning with $2S+1 = 26$, the electronic states are ferromagnetic, and the lowest ferromagnetic isomer found ($2S+1 = 30$) is shown in Figure 5. Unlike the low-lying ferrimagnetic states, the lowest ferromagnetic state is a capped octahedron.

The ground states of Mn_7^- and Mn_7^+ are pentagonal bipyramids as found for the neutral, and they obey the "± 1 rule". The ferromagnetic states of the ions are significantly above

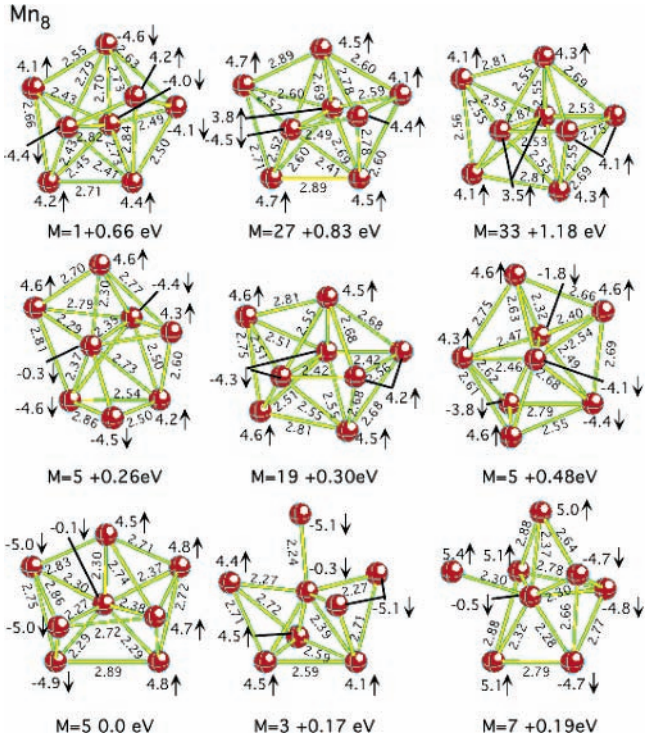

Figure 6. Optimized states of Mn_8.

the ferrimagnetic states, and they are also capped octahedrons, as in the neutral.

6. Mn_8, Mn_8^-, and Mn_8^+. For Mn_8, we present, in Figure 6, the lowest-energy ferrimagnetic 4:4. 2:6, and 1:7 states, as well as the lowest-energy ferromagnetic state. The ground state has the spin multiplicity of $2S+1 = 5$ and possesses a strongly distorted capped pentagonal bipyramid geometry. The computed magnetic moment per atom for the ground state is 0.5 μ_b, which is smaller than the experimental value[12] of 1.04 ± 0.14 μ_b. Our excess spin-down spin densities are located on the same atoms as found in the previous work.[9] The $2S+1 = 5$ isomers shown in Figure 6 have similar geometries, but they differ in the location and the value of the excess spin-down densities. As is seen, the changes in total energy due to different excess spin density couplings are small. This shows once more the difficulties associated with the study of ferrimagnetic states, namely, a large number of states with similar geometries and similar energies that differ only in the distribution of the excess spin densities.

As shown in Figure 6, many of the higher-energy structures are bicapped octahedrons. Interestingly, these include the ferromagnetic $2S+1 = 33$ state and an antiferromagnetic singlet. Both Mn_8^- and Mn_8^+ have a ground-state multiplicity of 4, i.e., they obey the "± 1 rule". The ground states of the ions are shown in Figure 7, and for both ions, their structures are more open than for the neutral ground state.

7. Mn_9, Mn_9^-, and Mn_9^+. We find Mn_9 to have a doublet ground state. The magnetic moment per atom for the ground state is 0.11 μ_b, which is much smaller than the experimental value[12] of 1.01 ± 0.10 μ_b. Our value is in disagreement with the previous theoretical work[9] that predicts a $2S+1 = 10$ state to be the lowest one. However, it should be noted that their search was restricted to spin states that were consistent with experiment. We find the $2S+1 = 10$ and $2S+1 = 12$ states to be 0.22 eV above the ground state. The low-energy isomers presented in Figure 8 have geometries that might be best viewed as arising by adding two Mn atoms to a distorted pentagonal

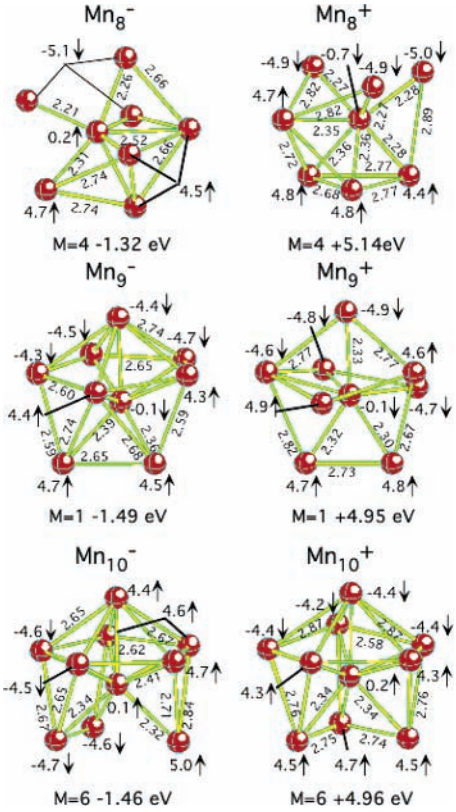

Figure 7. Optimized ground states of the Mn_8, Mn_9^- and Mn_{10} ions.

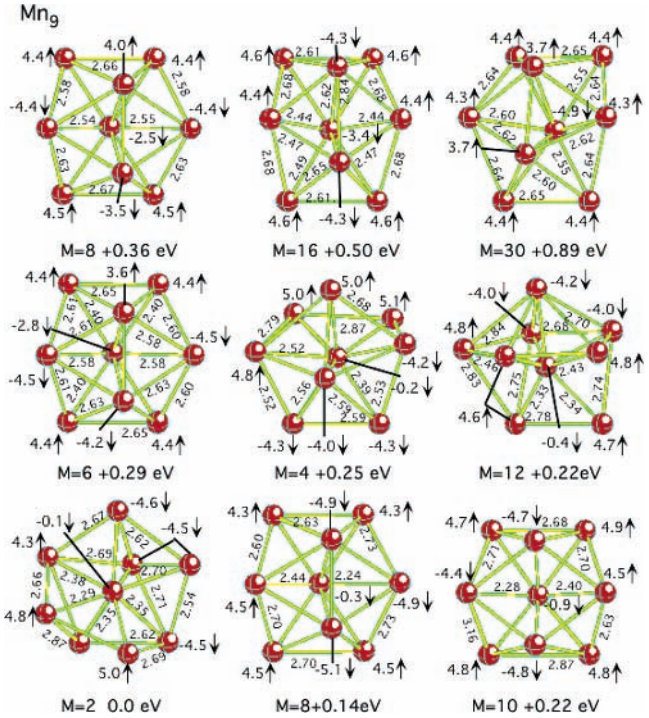

Figure 8. Optimized states of Mn_9.

bipyramid. The "hub" atom has the shortest distances to all other atoms and carries very little excess density in the ground state.

We find the ground states of Mn_9^- and Mn_9^+ to be the singlets, which is consistent with the "± 1 rule". Their first excited states are triplets, which are above the ground states by 0.24 and 0.11 eV, respectively. The ground-state geometries of the neutral in Figure 8, and the ions in Figure 7 have similar shapes.

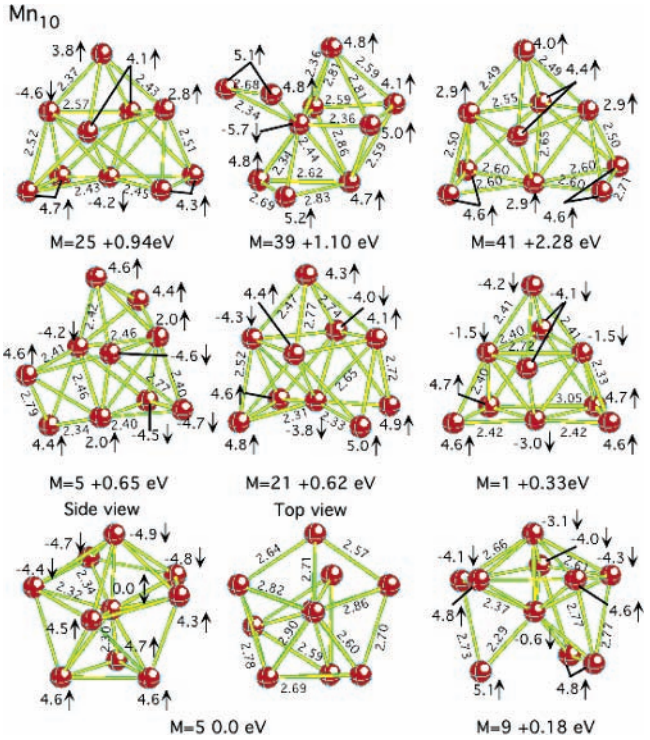

Figure 9. Optimized states of Mn_{10}.

8. Mn_{10}, Mn_{10}^-, and Mn_{10}^+. The geometrical structure of Mn_{10} is a distorted pentagonal bipyramid with a triangle of atoms attached, see Figure 9. The ground state has the spin multiplicity of 5 that corresponds to the total magnetic moment per atom of 0.4 μ_B, which is substantially smaller than the experimentally deduced[12] value of 1.34 ± 0.09 μ_B. The experimental value corresponds to states with 2S+1 = 11, 13, or 15. Our intensive search found only one low-lying 4:5 state with 2S+1 = 7 that is 0.07 eV above the ground state; the spin coupling in this excited state is similar to that in the ground state except that the excess spin density (0.7 *e*) on the hub atom is larger for the excited state. Figure 9 shows selected optimized states that correspond to the lowest energy ferrimagnetic states with different excess spin density orderings, a 2S+1 = 5 isomer, and the lowest-energy ferromagnetic state. There is a strong dependence of the geometry on the change in the excess spin density ordering, which resulted in a number of transition states during the geometry optimization process, again demonstrating the complexity of studying ferrimagnetic states. The geometry of the ferromagnetic state is a tetra-capped octahedron; this state is 2.28 eV above the ground state.

We find the ground states of both the cation and anion to have a spin multiplicity of 6. Thus, Mn_{10}^- and Mn_{10}^+ follow the "±1 rule". Both Mn_{10}^- and Mn_{10}^+ have very low-lying states with a spin multiplicity of 4; these are 0.01 and 0.04 eV above the ground states, respectively.

A common feature of the structures shown in Figures 3−9 is that the atoms with excess spin-up and excess spin-down spin densities form two interconnected graphs. This connectivity is related to a specific chemical bonding, as was mentioned above. Consider the case of the excess spin-up density atoms. Their chemically inert 3d-subshells contribute to the excess spin-up densities and the bonding is due to 4s spin-up and hybrid 3d4s spin-down densities. The opposite is true for the atoms with the excess spin-down densities. Thus the atoms with parallel excess spin density are adjacent to maximize the bonding. The central or "hub" atom plays a dual role and bonds to both types of atoms. All of its 3d and 4s electrons participate in the bonding, which leaves the hub atom with nearly no excess spin density. A similar separation of the spin-up and spin down densities into connected sets was found[11] for Mn_{15}, Mn_{19}, and Mn_{23}.

TABLE 1: Harmonic Vibrational Frequencies of the Ground-State Mn_n Clusters

n	frequencies (cm^{-1})
3	137, 137, 201
4	139, 139, 169, 169, 169, 229
5	71, 101, 141, 142, 148, 154, 170, 212, 231
6	82, 88, 95, 120, 131, 152, 167, 169, 187, 194, 216, 234
7	80, 83, 112, 118, 123, 128, 135, 140, 154, 165, 168, 175, 210, 211, 227
8	32, 56, 85, 89, 97, 104, 115, 132, 142, 152, 159, 184, 190, 196, 226, 272, 310, 351
9	24, 48, 55, 76, 103, 109, 111, 121, 124, 130, 141, 145, 159, 171, 183, 189, 204, 215, 279, 289, 331
10	24, 47, 58, 78, 87, 91, 94, 100, 113, 121, 128, 134, 140, 158, 161, 167, 179, 188, 196, 204, 223, 281, 311, 337

B. Frequencies and Electronic Properties. Harmonic vibrational frequencies of the ground states of the neutral Mn_n clusters are presented in Table 1. The resonance Raman spectrum was measured[45] for Mn_3 trapped in argon and krypton matrices, with ω_a reported as 130 cm^{-1} and $\omega_s - 2x_s$ as 197 cm^{-1}. Unfortunately independent values of ω_s and x_s could not be obtained. However, despite these limitations, there appears to be reasonable agreement between theory (ω_a = 131 and ω_s = 201 cm^{-1}) and experiment.

It is interesting to compare the frequencies of the Mn_{10} cluster to those of the Fe_{10} ground state, which has the spin multiplicity of 31. The Fe_{10} frequencies are found[46] to be: 39, 56, 74, 83, 122, 140, 153, 155, 159, 160, 180, 187, 188, 195, 203, 209, 216, 241, 245, 251, 259, 299, 331, and 336 cm^{-1}. One can see that the largest frequencies are nearly the same for Mn_{10} and Fe_{10}, whereas the lowest frequency of Fe_{10} is almost twice that of Mn_{10} (24 cm^{-1}), probably reflecting the greater thermodynamic stability of Fe_{10}.

Our computed adiabatic electron affinities (see Table 2) reach the maximum at Mn_4(1.64 eV) and the minimum at Mn_3(1.27 eV). The EA_{ad}s for *n* = 5−10 are rather similar, and the difference between them does not exceed 0.1 eV. The positions of peaks in the photoelectron spectra[47] of Mn_5 and Mn_6 are at higher values of 1.5 and 1.7 eV, respectively, which are similar to our adiabatic values. Our computed adiabatic ionization energies decrease gradually with increasing *n*, beginning with Mn_6, see Table 2. The corresponding vertical detachment energies are in good agreement with the experimental data, except for Mn_8, where our adiabatic value is closer to the experimental value. The IE_{ad}s of Mn_9 and Mn_{10} are getting close to the photoelectric work function[48] of 4.1 ± 0.2 eV measured for the bulk Mn.

C. Thermodynamic Stability. Detachment of a single Mn atom corresponds to the lowest-energy dissociation channel for all neutral and charged Mn_n clusters as shown in Table 3. Except for the smaller clusters with *n* = 3−5, these energies are similar and do not depend significantly on the cluster charge. For example, in the Mn_{10} series, the difference in the Mn dissociation energy differs by 0.03 eV only. The near independence of the Mn dissociation energies on the cluster size may be related to the specific chemical bonding in the Mn_n cluster, namely the addition of one Mn atom to a Mn_n cluster generally leads to formation of 2 bonds because the effective atomic configuration of the Mn atom in the cluster is close to $3d^64s^1$. Experimental data are available[27,28] for the Mn_n^+−Mn channels with *n* =

TABLE 2: Adiabaitic Electron Affinities (EA_{Ad}) and Ionization Energies (IE_{Ad}) along with Vertical Ionization Energies (IE_{Vert}) of Mn_n Clusters[a]

	spin multiplicity								
	neutral	anion	cation	EA_{ad} TW	EA_{ad} Expl[b]	IE_{ad} TW	IE_{vert} LS[b]	IE_{vert} HS[b]	IE_{vert} Expl[c]
Mn_3	16	17	5	1.27		5.77	6.27	6.42	
Mn_4	21	20	10	1.64		5.86	6.42	6.67	
Mn_5	4	23	5	1.36	1.5	5.44	5.90	5.75	
Mn_6	9	8	8	1.42	1.7	5.58	5.86	5.66	
Mn_7	6	5	7	1.43		5.31	5.70	5.39	5.44 ± 0.05
Mn_8	5	4	4	1.32		5.14	5.41	5.42	4.91 ± 0.05
Mn_9	2	1	1	1.49		4.95	5.14	5.28	5.06 ± 0.05
Mn_{10}	5	6	6	1.46		4.94	5.06	5.08	5.26 ± 0.05

[a] All values are in eV. LS = 2S−1 and HS = 2S+3 designate the cation states formed by ionization of the corresponding ground-state neutral with the spin multiplicity of 2S+1. [b] See ref 47. [c] See ref 24.

TABLE 3: Computed Fragmentation Energies (in eV) of Neutral and Charged Mn_n[a]

neutral		anion		cation	
channel	TW	channel	TW	channel	TW (exp[b,c])
$Mn_3 \rightarrow Mn_2+Mn$	**1.41**	$Mn_3^- \rightarrow Mn_2^-+Mn$	**2.06**	$Mn_3^+ \rightarrow Mn_2^++Mn$	**1.85 (0.83 ± 0.05)**[b]
$Mn_4 \rightarrow Mn_3+Mn$	**2.24**	$Mn_4^- \rightarrow Mn_3^-+Mn$	**2.54**	$Mn_4^+ \rightarrow Mn_3^++Mn$	**2.08 (1.04 ± 0.07)**[b]
$\rightarrow 2Mn_2$	2.45	$\rightarrow Mn_2^-+Mn_2$	3.50	$\rightarrow Mn_2^++Mn_2$	2.84
$Mn_5 \rightarrow Mn_4+Mn$	**2.14**	$Mn_5^- \rightarrow Mn_4^-+Mn$	**1.87**	$Mn_5^+ \rightarrow Mn_4^++Mn$	**2.56 (1.70 ± 0.08)**[c]
$\rightarrow Mn_3+Mn_2$	3.21	$\rightarrow Mn_3^-+Mn_2$	3.30	$\rightarrow Mn_3^++Mn_2$	3.54
$Mn_6 \rightarrow Mn_5+Mn$	**2.33**	$Mn_6^- \rightarrow Mn_5^-+Mn$	**2.30**	$Mn_6^+ \rightarrow Mn_5^++Mn$	**2.43 (1.04 ± 0.10)**[c]
$\rightarrow Mn_4+Mn_2$	3.29	$\rightarrow Mn_4^-+Mn_2$	3.06	$\rightarrow Mn_4^++Mn_2$	3.56
$\rightarrow 2Mn_3$	4.08	$\rightarrow Mn_3^-+Mn_3$	4.22	$\rightarrow Mn_3^++Mn_3$	4.27
$Mn_7 \rightarrow Mn_6+Mn$	**2.31**	$Mn_7^- \rightarrow Mn_6^-+Mn$	**2.32**	$Mn_7^+ \rightarrow Mn_6^++Mn$	**2.58(1.46 ± 0.11)**[c]
$\rightarrow Mn_5+Mn_2$	3.54	$\rightarrow Mn_5^-+Mn_2$	3.52	$\rightarrow Mn_5^++Mn_2$	3.91
$\rightarrow Mn_4+Mn_3$	4.22	$\rightarrow Mn_4^-+Mn_3$	4.01	$\rightarrow Mn_4^++Mn_3$	4.77
$Mn_8 \rightarrow Mn_7+Mn$	**2.60**	$Mn_8^- \rightarrow Mn_7^-+Mn$	**2.50**	$Mn_8^+ \rightarrow Mn_7^++Mn$	**2.77**
$\rightarrow Mn_6+Mn_2$	3.81	$\rightarrow Mn_6^-+Mn_2$	3.72	$\rightarrow Mn_6^++Mn_2$	4.27
$\rightarrow Mn_5+Mn_3$	4.76	$\rightarrow Mn_5^-+Mn_3$	4.64	$\rightarrow Mn_5^++Mn_3$	5.32
$Mn_9 \rightarrow Mn_8+Mn$	**2.48**	$Mn_9^- \rightarrow Mn_8^-+Mn$	**2.64**	$Mn_9^+ \rightarrow Mn_8^++Mn$	**2.66**
$\rightarrow Mn_7+Mn_2$	3.98	$\rightarrow Mn_7^-+Mn_2$	4.04	$\rightarrow Mn_7^++Mn_2$	4.34
$\rightarrow Mn_6+Mn_3$	4.91	$\rightarrow Mn_6^-+Mn_3$	4.98	$\rightarrow Mn_6^++Mn_3$	5.54
$Mn_{10} \rightarrow Mn_9+Mn$	**2.43**	$Mn_{10}^- \rightarrow Mn_9^-+Mn$	**2.40**	$Mn_{10}^+ \rightarrow Mn_9^++Mn$	**2.43**
$\rightarrow Mn_8+Mn_2$	3.80	$\rightarrow Mn_8^-+Mn_2$	3.94	$\rightarrow Mn_8^++Mn_2$	3.98
$\rightarrow Mn_7+Mn_3$	4.90	$\rightarrow Mn_7^-+Mn_3$	5.05	$\rightarrow Mn_7^++Mn_3$	5.39

[a] Dissociation energies of Mn_2, Mn_2^-, and Mn_2^+ computed at the BPW91/6-311+G* level are 1.15, 1.69, and 1.91 eV, respectively, see refs 25, 39. [b] See ref 27. [c] See ref 28.

2−7, and as is rather usual, the DFT values are overestimated by about 1 eV. One may anticipate that the computational error is systematic and the trends in relative stability in the neutral and charged Mn_n clusters are reproduced correctly. The fragmentation energies involving the loss of Mn_2 and Mn_3 are appreciably larger and show less uniformity than the loss of a single Mn atom.

IV. Summary and Conclusions

In the present work, we performed DFT-GGA optimizations of the Mn_n, Mn_n^-, and Mn_n^+ series for $n = 3-10$ considering all possible spin states for all three series. The optimization process was rather complete, starting from the highest spin state possible and lowering the spin of the states in steps. Tests were performed where the spin was increased or where the lowest total energy states obtained in each series were used as the guesses for additional searches of the lowest energy states in the two other series. However, even such a time-consuming strategy does not guarantee that the lowest energy states found correspond to the global minima of the corresponding species. The problem is that there are many different spin couplings of the nonbonding 3d orbitals (excess spin density coupling schemes) for ferrimagnetic states. Their search is complicated because we cannot flip excess spin densities on a specific atom directly, but instead must search indirectly for different solutions by increasing or decreasing the distances between atoms of existing solutions.

Ferrimagnetic states, i.e., the states in which the excess spin densities at some atoms are antiferromagnetically coupled to the excess spin densities at the other atoms, are the ground states beginning with Mn_5. The energy difference between ferrimagnetic and ferromagnetic states grows rapidly and exceeds 2 eV in Mn_{10}. The switch from ferromagnetic to ferrimagnetic ground state occurs at Mn_6^- and Mn_3^+ in the corresponding anionic and cationic series. This is related to a specific chemical bonding in ferrimagnetic states that allows the formation of hybrid 3d4s bonds in the both spin representations. The sets of atoms with spin-up and spin-down excess spin densities form two connected sets. These sets are bonded by delocalized orbitals that are primarily 4s in the character in the smaller species, whereas in the larger clusters, in addition to the delocalized 4s bonding, a central atom forms bonds in both spin representation. This atom carries no excess spin density because it forms the α-bonds with one connected set and the β-bonds with the other one. Previously, we have found a similar bonding mechanism[49] in the ferrimagnetic ($Fe^{\uparrow}$ − C − $Fe^{\downarrow}$) ground $^2\Delta$ state of Fe_2C,

where the carbon atom forms β-bonds with the left-hand Fe atom and α-bonds with the right-hand Fe atom.

The effective atomic electronic configuration of Mn in the clusters grows from $3d^{5.5}4s^{1.5}$ in the smaller clusters to close to $3d^64s^1$ in the larger clusters. Adding an Mn atom to a Mn_n cluster allow the formation of 2 bonds, which results in very similar binding energies for an Mn atom that is nearly independent of the cluster size or its charge state, except for the smallest clusters. The neutral clusters possess similar adiabatic electron affinities and ionization energies.

Acknowledgment. This work was supported in part by the Army High Performance Computing Research Center (AHPCRC) under the auspices of the Department of the Army, Army Research Laboratory (ARL) under Cooperative Agreement number DAAD19-01-2-0014. The content of this manuscript does not necessarily reflect the position or the policy of the government, and no official endorsement should be inferred.

References and Notes

(1) Hobbs, D.; Hafner, J.; Spišák, D. *Phys. Rev. B: Condens. Matter Mater. Phys.* **2003**, *68*, 014407.

(2) Van Zee, R. J.; Baumann, C. A.; Bhat, S. V.; Weltner, W., Jr. *J. Chem. Phys.* **1982**, *76*, 5636.

(3) Baumann, C. A.; Van Zee, R. J.; Bhat, S. V.; Weltner, W., Jr. *J. Chem. Phys.* **1983**, *78*, 190.

(4) Nayak, S. K.; Jena, P. *Chem. Phys. Lett.* **1998**, *289*, 473.

(5) Pederson, M. R.; Reuse, F.; Khanna, S. N. *Phys. Rev. B: Condens. Matter Mater. Phys.* **1998**, *58*, 5632.

(6) Bobadova-Parvanova, P.; Jackson, K. A.; Srinivas, S.; Horoi, M. *Phys. Rev. A: At., Mol., Opt. Phys.* **2003**, *67*, 061202.

(7) Jones, N. O.; Khanna, S. N.; Baruah, T.; Pederson, M. R. *Phys. Rev. B: Condens. Matter Mater. Phys.* **2004**, *70*, 045416.

(8) Khanna, S. N.; Rao, B. K.; Jena, P.; Knickelbein, M. *Chem. Phys. Lett.* **2003**, *378*, 374.

(9) Bobadova-Parvanova, P.; Jackson, K. A.; Srinivas, S.; Horoi, M. *J. Chem. Phys.* **2005**, *122*, 014310.

(10) Nayak, S. K.; Nooijen, M.; Jena, P. *J. Phys. Chem. A* **1999**, *103*, 9853.

(11) Briere, T. M.; Sluiter, M. H. F.; Kumar, V.; Kawazoe, Y. *Phys. Rev. B: Condens. Matter Mater. Phys.* **2002**, *66*, 064412.

(12) Knickelbein, M. B., *Phys. Rev. B: Condens. Matter Mater. Phys.* **2004**, *70*, 014424.

(13) Sandratskii, L. M.; Guletskii, P. G. *J. Phys. F: Met. Phys.* **1986**, *16*, L43.

(14) Kübler, J.; Hock, K.-H.; Sticht, J.; Williams, A. R. *J. Phys. F: Met. Phys.* **1988**, *18*, 469.

(15) Longo, R. C.; Noya, E. G.; Gallego, L. J. *J. Chem. Phys.* **2005**, *122*, 226102.

(16) Longo, R. C.; Noya, E. G.; Gallego, L. J. *Phys. Rev. B: Condens. Matter Mater. Phys.* **2005**, *72*, 174409.

(17) Hobbs, D.; Kresse, G.; Hafner, J. *Phys. Rev. B: Condens. Matter Mater. Phys.* **2000**, *62*, 11566.

(18) Rollmann, G.; Entel, P.; Sahoo, S. *Comput. Mater. Sci.* **2006**, *35*, 275.

(19) Ohno, H. *Science* **1998**, *281*, 951.

(20) Dietl, T.; Ohno, H.; Matsukura, F.; Cibert, J.; Ferrand, D. *Science* **2000**, *287*, 1019.

(21) Konig, J.; Lin, H.; MacDonald, A. *Phys. Rev. Lett.* **2000**, *84*, 5628.

(22) Litvinov, V.; Dugaev, V. *Phys. Rev. Lett.* **2001**, *86*, 5593.

(23) Raebiger, H.; Ayuela, A.; von Boehm, *Phys. Rev. B: Condens. Matter Mater. Phys.* **2005**, *72*, 014465.

(24) Koretsky, G. M.; Knickelbein, M. B. *J. Chem. Phys.* **1997**, *106*, 9810.

(25) Gutsev, G. L.; Bauschlicher, C. W., Jr. *J. Phys. Chem. A* **2003**, *107*, 4755.

(26) Terasaki, A.; Briere, T. M.; Kulawik, M.; Minemoto, S.; Tono, K.; Matsushita, A.; Kondow, T. *J. Chem. Phys.* **2003**, *118*, 2180.

(27) Terasaki, A.; Minemoto, S.; Kondow, T. *J. Chem. Phys.* **2002**, *117*, 7520.

(28) Tono, K.; Terasaki, A.; Ohta, T.; Kondow, T. *J. Chem. Phys.* **2005**, *123*, 174314.

(29) Frisch, M. J.; Trucks, G. W.; Schlegel, H. B.; Scuseria, G. E.; Robb, M. A.; Cheeseman, J. R.; Zakrzewski, V. G.; Montgomery, J. A., Jr.; Stratmann, R. E.; Burant, J. C.; Dapprich, S.; Millam, J. M.; Daniels, A. D.; Kudin, K. N.; Strain, M. C.; Farkas, O.; Tomasi, J.; Barone, V.; Cossi, M.; Cammi, R.; Mennucci, B.; Pomelli, C.; Adamo, C.; Clifford, S.; Ochterski, J.; Petersson, G. A.; Ayala, P. Y.; Cui, Q.; Morokuma, K.; Malick, D. K.; Rabuck, A. D.; Raghavachari, K.; Foresman, J. B.; Cioslowski, J.; Ortiz, J. V.; Stefanov, B. B.; Liu, G.; Liashenko, A.; Piskorz, P.; Komaromi, I.; Gomperts, R.; Martin, R. L.; Fox, D. J.; Keith, T.; Al-Laham, M. A.; Peng, C. Y.; Nanayakkara, A.; Gonzalez, C.; Challacombe, M.; Gill, P. M. W.; Johnson, B. G.; Chen, W.; Wong, M. W.; Andres, J. L.; Head-Gordon, M.; Replogle, E. S.; Pople, J. A. *Gaussian 98*, revision A.11; Gaussian, Inc.: Pittsburgh, PA, 2001.

(30) Frisch, M. J.; Trucks, G. W.; Schlegel, H. B.; Scuseria, G. E.; Robb, M. A.; Cheeseman, J. R.; Montgomery, J. A., Jr.; Vreven, T.; Kudin, K. N.; Burant, J. C.; Millam, J. M.; Iyengar, S. S.; Tomasi, J.; Barone, V.; Mennucci, B.; Cossi, M.; Scalmani, G.; Rega, N.; Petersson, G. A.; Nakatsuji, H.; Hada, M.; Ehara, M.; Toyota, K.; Fukuda, R.; Hasegawa, J.; Ishida, M.; Nakajima, T.; Honda, Y.; Kitao, O.; Nakai, H.; Klene, M.; Li, X.; Knox, J. E.; Hratchian, H. P.; Cross, J. B.; Bakken, V.; Adamo, C.; Jaramillo, J.; Gomperts, R.; Stratmann, R. E.; Yazyev, O.; Austin, A. J.; Cammi, R.; Pomelli, C.; Ochterski, J. W.; Ayala, P. Y.; Morokuma, K.; Voth, G. A.; Salvador, P.; Dannenberg, J. J.; Zakrzewski, V. G.; Dapprich, S.; Daniels, A. D.; Strain, M. C.; Farkas, O.; Malick, D. K.; Rabuck, A. D.; Raghavachari, K.; Foresman, J. B.; Ortiz, J. V.; Cui, Q.; Baboul, A. G.; Clifford, S.; Cioslowski, J.; Stefanov, B. B.; Liu, G.; Liashenko, A.; Piskorz, P.; Komaromi, I.; Martin, R. L.; Fox, D. J.; Keith, T.; Al-Laham, M. A.; Peng, C. Y.; Nanayakkara, A.; Challacombe, M.; Gill, P. M. W.; Johnson, B.; Chen, W.; Wong, M. W.; Gonzalez, C.; Pople, J. A. *Gaussian 03*, revision B.05; Gaussian, Inc.: Pittsburgh, PA, 2003.

(31) Wachters, A. J. H. *J. Chem. Phys.* **1970**, *52*, 1033.

(32) Hay, P. J. *J. Chem. Phys.* **1977**, *66*, 4377.

(33) Frisch, M. J.; Pople, J. A.; Binkley, J. S. *J. Chem. Phys.* **1984**, *80*, 3265.

(34) Raghavachari, K.; Trucks, G. W. *J. Chem. Phys.* **1989**, *91*, 1062.

(35) Becke, A. D. *Phys. Rev. A* **1988**, *38*, 3098.

(36) Perdew, J. P.; Wang, Y. *Phys. Rev. B: Condens. Matter Mater. Phys.* **1992**, *45*, 13244.

(37) Gutsev, G. L.; Bauschlicher, C. W., Jr. *J. Phys. Chem. A* **2003**, *107*, 7013.

(38) Mulliken, R. S. *J. Chem. Phys.* **1955**, *23*, **1833**, *1841*, 2338, 2343.

(39) Reed, A. E.; Curtiss, L. A.; Weinhold, F. *Chem. Rev.* **1988**, *88*, 899.

(40) Gutsev, G. L.; Mochena, M. D.; Jena, P.; Bauschlicher, C. W., Jr.; Partridge, H., III *J. Chem. Phys.* **2004**, *121*, 6785.

(41) Morse, M. D. *Advances in Metal and Semiconductor Clusters*; JAI Press Inc.: Greenwich, CT, 1993; Vol. 1, pp 83−121.

(42) Yamamoto, S.; Tatewaki, H.; Moriyama, H.; Nakano, M. *J. Chem. Phys* **2006**, *124*, 124302.

(43) Papas, B. N.; Schaefer, H. F., III *J. Chem. Phys.* **2005**, *123*, 074321.

(44) Furche, F.; Perdew, J. P. *J. Chem. Phys.* **2006**, *124*, 044103.

(45) Bier, K. D.; Haslett, T. L.; Kirkwood, A. D.; Moskowitz, M. *J. Chem. Phys.* **1988**, *89*, 6.

(46) Gutsev, G. L.; Mochena, M. D.; Bauschlicher, C. W., Jr. To be submitted.

(47) Bowen, K. *reference [9]* in ref 7.

(48) Eastman, D. E. *Phys. Rev.* **1970**, *2*, 1.

(49) Gutsev, G. L.; Bauschlicher, C. W., Jr. *Chem. Phys.* **2003**, *291*, 27.